JOURNAL OF VIROLOGY, Aug. 2008, p. 8138–8148 Vol. 82, No. 16
0022-538X/08/$08.00+0 doi:10.1128/JVI.00368-08

Mutagenesis and Nuclear Magnetic Resonance Analyses of the Fusion Peptide of *Helicoverpa armigera* Single Nucleocapsid Nucleopolyhedrovirus F Protein▽

Ying Tan,[1,3] Ling Jiang,[2] Manli Wang,[1,3] Feifei Yin,[1,3] Fei Deng,[1] Maili Liu,[2] Zhihong Hu,[1] and Hualin Wang[1]*

State Key Laboratory of Virology and Joint Laboratory of Invertebrate Virology, Wuhan Institute of Virology, Chinese Academy of Sciences, Wuhan 430071, People's Republic of China[1]; State Key Laboratory of Magnetic Resonance and Atomic and Molecular Physics, Wuhan Institute of Physics and Mathematics, Chinese Academy of Sciences, Wuhan 430071, People's Republic of China[2]; and Graduate School of the Chinese Academy of Sciences, Beijing 100039, People's Republic of China[3]

Received 19 February 2008/Accepted 28 May 2008

The entry of enveloped viruses into cells is normally mediated by fusion between viral and cellular membranes, in which the fusion peptide plays a crucial role. The fusion peptides of group II nucleopolyhedrovirus (NPV) F proteins are quite conserved, with a hydrophobic region located at the N terminal of the F_1 fragment. For this report, we used mutagenesis and nuclear magnetic resonance (NMR) to study the structure and function of the fusion peptide of the *Helicoverpa armigera* single-nucleocapsid NPV (HearNPV) F protein (HaF). Five mutations in the fusion peptide of HaF, N^1G, N^1L, I^2N, G^3L, and $D^{11}L$, were generated separately, and the mutated *f* genes were transformed into the *f*-null HearNPV bacmid. The mutations N^1L, I^2N, and $D^{11}L$ were found to completely abolish the ability of the recombinant bacmids to produce infectious budded virus, while the mutations N^1G and G^3L did not. The low-pH-induced envelope fusion assay demonstrated that the N^1G substitution increased the fusogenicity of HaF, while the G^3L substitution reduced its fusogenicity. NMR spectroscopy was used to determine the structure of a synthetic fusion peptide of HaF in the presence of sodium dodecyl sulfate micelles at pH 5.0. The fusion peptide appeared to be an amphiphilic structure composed of a flexible coil in the N terminus from N^1 to N^5, a 3_{10}-helix from F^6 to G^8, a turn at S^9, and a regular α-helix from V^{10} to D^{19}. The data provide the first NMR structure of a baculovirus fusion peptide and allow us to further understand the relationship of structure and function of the fusion peptide.

The penetration of an enveloped virus into a host cell requires fusion of the viral envelope and host cellular membrane to release the viral genome and accessory proteins into the host cell after appropriate receptor recognition. The fusion process is catalyzed by specialized viral fusion glycoproteins that can be separated into two classes, I and II, depending on their structures (24–26, 43). A common feature of all viral fusion proteins is that they contain a highly conserved hydrophobic sequence termed the "fusion peptide" which plays a central role in facilitating membrane fusion. After a triggering event, such as a change in pH or binding to a receptor, the fusion protein undergoes a large conformational change that allows the fusion peptide to be exposed and inserted into the target membrane (11, 48). The insertion of the fusion peptide induces membrane deformation to such an extent that it fuses with another membrane that has been brought into close proximity by the ectodomain of the fusion protein (12, 44, 52). Therefore, how fusion peptides interact with host membranes has long been of great interest. The three-dimensional structure of the fusion peptide is essential to understanding this mechanism. Some of the structures of fusion peptides of different viruses, such as the fusion peptide of influenza virus hemagglutinin (HA) (16, 28) and the fusion peptide of HIV gp41 (7, 23, 30, 42), have been determined by nuclear magnetic resonance (NMR) and other techniques.

The *Baculoviridae* family contains two genera, *Nucleopolyhedrovirus* (NPV) and *Granulovirus*. The NPVs are subdivided into group I and group II based on phylogenetic analyses (5, 18, 55). Two types of envelope fusion protein have been identified in the budded virus (BV) of baculoviruses. In group I NPVs, the process of viral attachment, low-pH-dependent membrane fusion, and viral budding is mediated by the envelope glycoprotein GP64 (3, 17, 36, 37). Another type of membrane fusion protein, called F protein, has been identified in more-diversely differentiated group II NPVs, such as LD130 of *Lymantria dispar* multiple-nucleocapsid NPV (MNPV) (38), SE8 of *Spodoptera exigua* MNPV (22), and HA133 of *Helicoverpa armigera* single-nucleocapsid NPV (HearNPV) (HaF) (33). F proteins are responsible for binding the virus to cells and mediating the fusion of viral and endosomal membranes following endocytosis, as well as the budding process (39, 49, 50). The F protein is synthesized as a precursor (F_0) and then cleaved by a subtilisin-like proprotein convertase (furin) to form the active protein that consists of the disulfide-linked chains F_1 and F_2, resulting in the release of the fusion peptide in the N terminus of F_1 (51) (Fig. 1A). The fusion peptide of F protein shares general features with those of many other viral fusion proteins, which tend to be rich in glycine residues and can be modeled as sided helices with the bulky apolar

* Corresponding author. Mailing address: Wuhan Institute of Virology, Chinese Academy of Sciences, Wuhan 430071, People's Republic of China. Phone and fax: 86-27-87199353. E-mail: h.wang@wh.iov.cn.
▽ Published ahead of print on 4 June 2008.

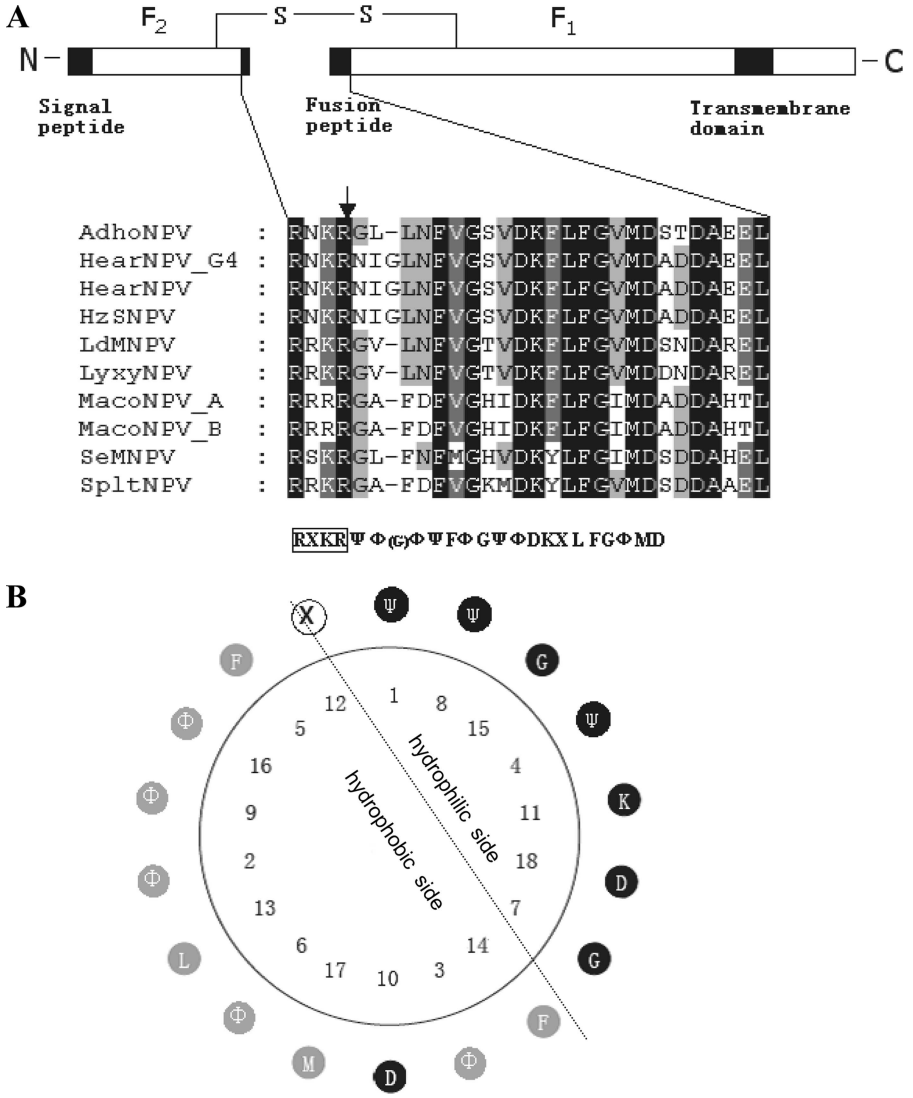

FIG. 1. Presentation of group II F protein and fusion peptides. (A) Schematic presentation of group II F protein and multiple sequence alignment of the putative fusion peptides. The line represents the disulfide-linked F protein subunits F_1 and F_2. The signal peptide, fusion peptide, and transmembrane domain are represented by black boxes. The expanded section shows a comparison of the amino acid sequences of the fusion peptides of group II F proteins. Alignment columns are shaded according to conservation (black, 100% identity; gray, 60 to 80% identity). Below the alignment is the consensus sequence. Ψ represents hydrophilic amino acids, Φ represents hydrophobic amino acids, X represents any amino acid, and G in the parentheses represents the extra amino acid in the fusion peptides of HearNPV and HzNPV. The consensus furin recognition sequence is boxed, and the arrow indicates the cleavage site. (B) Helical wheel presentation of the putative fusion peptide of group II NPV F proteins. Hydrophilic residues are shown in black, hydrophobic residues are shown in gray, and any residues in white. The simplest amino acid G with an "–H" side chain is classified as hydrophilic. The dotted line represents the division between the hydrophilic face and the hydrophobic face of the amphiphilic residues. The fusion peptide is numbered from the N terminus of the cleaved F_1 fragment.

residues on one face of the helix (45). However, to our knowledge, there is no report of the detailed structure of the baculovirus fusion peptide.

An alignment of fusion peptides of the F proteins from different group II NPVs revealed a consensus sequence of "ΨΦ(G)ΦΨFΦGΨΦDKXLFGΦMD," where Ψ represents hydrophilic amino acids, Φ represents hydrophobic amino acids, X represents any amino acids, and G in the blanket represents the extra amino acid in the fusion peptides of HearNPV and *Helicoverpa zea* single-nucleocapsid NPV (HzSNPV) (Fig. 1A). The typical fusion peptide of group II NPVs can be modeled as an amphiphilic helix with a highly hydrophobic face and a highly hydrophilic face (Fig. 1B). Several experimental mutations have been introduced into this region to investigate the role of certain amino acids in the structure and function of the fusion peptide. For example, some hydrophilic or hydrophobic substitutions in the fusion peptide of SE8 impaired virus propagation, and the mutagenesis of $K^{158}A$, $D^{165}G$, and $D^{168}G$ of the fusion peptide of LD130 resulted in reduction of its fusion ability (39, 50).

The fusion peptide of HaF is different from those of other group II F proteins (except for HzSNPV) in that it contains an extra glycine (G^3). Consequently, the predicted amphiphilic helix of the fusion peptide of HaF (Fig. 2) is also different from

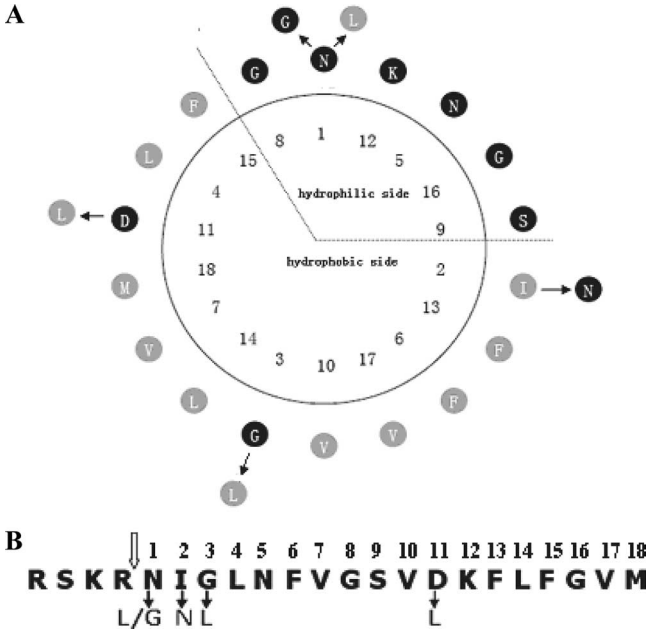

FIG. 2. Presentation of the fusion peptide and mutations of HaF. (A) Helical-wheel presentation of the fusion peptide of HaF. Fusion peptide residues are numbered from the N terminus of the F_1 subunit. The mutations are indicated at the outside of the helical wheel with arrows and substituted amino acids. (B) Linear presentation of the fusion peptide of HaF (the first 18 N-terminal amino acids of the cleaved HearNPV F_1 fragment). The open arrow indicates the furin cleavage site. Solid arrows indicate amino acid changes for the mutations.

those of typical group II fusion peptides (Fig. 1B). For this report, we investigated the structure and function of the fusion peptide of HaF by using mutagenesis and NMR approaches. Several amino acids were mutated in order to study their effects on the function of the protein (Fig. 2). As it has been shown that the first residue of influenza hemagglutinin fusion peptide is important (40), the importance of the first hydrophilic asparagine (N^1) of the fusion peptide of HaF was verified by replacing it with either leucine or glycine. The hydrophobic isoleucine (I^2) at the edge of the hydrophobic side was replaced with hydrophilic asparagine. The extra glycine (G^3) was mutated to hydrophobic leucine. The hydrophilic aspartic acid (D^{11}) in the hydrophobic side of the helical wheel was replaced with hydrophobic leucine. The infectivity of the recombinant bacmids with the mutant *f* genes was assayed, and their fusogenicity and production of progeny virus were compared to those of the parental virus. Furthermore, NMR spectroscopy was used to determine the structure of a synthetic fusion peptide of HaF. The deduced NMR structure was used to better understand the relationship between structure and function of the fusion peptide.

MATERIALS AND METHODS

Insect cells and virus. HzAM1 cells (35) were maintained at 27°C in Grace's complete medium (Gibco-BRL) containing 10% fetal bovine serum, pH 6.0. An HearNPV bacmid, HaBacHZ8, and an *f*-null bacmid, HaBacΔF, were previously constructed in our laboratory (46, 47).

Computational analysis. Sequence alignments of fusion peptides were performed with DNAStar's MegAlign software and edited with Genedoc software. The helical-wheel projection was performed with ANTHEPROT software and the Protean software of DNAStar.

Construction of recombinant BVs with mutant HaFs. The HaF gene (*Ha133*) was amplified from HaBacHZ8 by using Pyrobest DNA polymerase (Takara) (46). The primers used were HaF-For (5′-GGGGAATTCATGGTTGCGATA AAAAGTAGTATG-3′) (EcoRI site underlined) and HaF-Rev (5′-CCCGAGC TCCGTAGGGATTTGCCGTCG-3′) (SacI site underlined). The PCR product was cloned into pGEM-T Easy (Promega) to generate the intermediate plasmid pT-HaF. Sequence analysis was used to confirm the correctness of the clone. Plasmid pFastBac1-Op166 was constructed by inserting the *gp64* promoter of *Orgyia pseudotsugata* MNPV (Op166) into the BamHI site of pFastBac1 (Bac-to-Bac baculovirus expression system; Gibco-BRL) (47). The HaF gene was digested from pT-HaF and inserted into pFastBac1-Op166 (digested with EcoRI and SacI) to generate the transfer plasmid pFastBac1-Op166-HaF.

Mutant HaF genes were generated by using overlap extension PCRs as described earlier (19). The mutagenic primers are listed in Table 1; Pyrobest DNA polymerase was used for all PCR amplifications. For generating HaF^{N1L}, pT-HaF was used as the template for the following two PCRs: one with HaF-For and HaF^{N1L} 3′ as primers and the other with HaF^{N1L} 5′ and HaF-Rev as primers (Table 1). Then, the PCR products were annealed to each other and the external primers HaF-For and HaF-Rev were used to generate the HaF^{N1L} gene. The HaF^{N1L} fragment generated was cloned into the pGEM-T Easy vector and verified by sequencing. The HaF^{N1L} fragment was then inserted into pFastBac1-Op166 to generate pFastBac1-Op166-HaF^{N1L}. Similarly, the other mutants, HaF^{N1G}, HaF^{I2N}, HaF^{G3L}, and HaF^{D11L}, were also generated and cloned into pFastBac1-Op166.

Each of the transfer plasmids (pFastBac1-Op166-HaF and the pFastBac1-Op166-HaF mutants) was transformed into competent DH10Bac cells containing HaBacΔF and the helper plasmid expressing transposase (Bac-to-Bac baculovirus expression system; Gibco-BRL). The transposition of inserts from transfer plasmids to HaBacΔF was confirmed by PCR using primer HaF-For in combination with the M13 reverse primer (5′-AGCGGATAACAATTTCACACA GG-3′) and the M13 forward primer (5′-CCCAGTCACGACGTTGTAAAACA-3′). The bacmids identified were designated HaBacΔF-HaF, HaBacΔF-HaF^{N1L}, HaBacΔF-HaF^{N1G}, HaBacΔF-HaF^{I2N}, HaBacΔF-HaF^{G3L}, and HaBacΔF-HaF^{D11L}, and their DNAs were purified for transfection assays.

Transfection and infection assays. For transfection, HzAM1 cells were seeded into 35-mm-diameter tissue culture dishes at a rate of 3×10^5 cells per dish. After 24 h, cells were transfected with approximately 1 μg of each bacmid DNA, using 12 μl Lipofectin reagent according to the Bac-to-Bac expression system's manual (Invitrogen). Supernatants were harvested at 6 days posttransfection (p.t.), and 1 ml of each supernatant was used to infect 1×10^6 HzAM1 cells. Transfected and infected cells were observed by fluorescence microscopy. The titers of the budded viruses were determined by end-point dilution assay, and progeny viruses were amplified by infecting 5×10^6 HzAM1 cells at a multiplicity of infection (MOI) of 0.1 50% tissue culture infective dose ($TCID_{50}$) U/cell.

TABLE 1. Nucleotide sequences of mutagenetic primers

Primer	Sequence (5′–3′)[a]
HaF^{N1L} 5′	.....CAACATTCTCGAGTCGCAACAAACGACTCA
	TTGGATTGAACTTCGTTGG
HaF^{N1L} 3′	.....CCAACGAAGTTCAATCCAATGCGTTTGTTG
	CGACTCGAGAATGTTG
HaF^{N1G} 5′	.....CAACATTCTCGAGTCGCAACAAACGAGGC
	ATTGGATTGAACTTCGTTGG
HaF^{N1G} 3′	.....CCAACGAAGTTCAATCCAATGCCTCGTTTG
	TTGCGACTCGAGAATGTTG
HaF^{I2N} 5′	.....CGAGTCGCAACAAACGAAACAACGGATTG
	AACTTCGTTGGAAG
HaF^{I2N} 3′	.....CTTCCAACGAAGTTCAATCCGTTGTTTCGTT
	TGTTGCGACTCG
HaF^{G3L} 5′	.....CGAGTCGCAACAAACGAAACATTCTCTTGA
	ACTTCGTTGGAAGCGTAGAC
HaF^{G3L} 3′	.....GTCTACGCTTCCAACGAAGTTCAAGAGAAT
	GTTTCGTTTGTTGCGACTCG
HaF^{D11L} 5′	.....GATTGAACTTCGTTGGAAGCGTATTGAAGT
	TTCTGTTTGGAGTGATG
HaF^{D11L} 3′	.....CATCACTCCAAACAGAAACTTCAATACGCT
	TCCAACGAAGTTCAATC

[a] Mutated nucleotides are underlined.

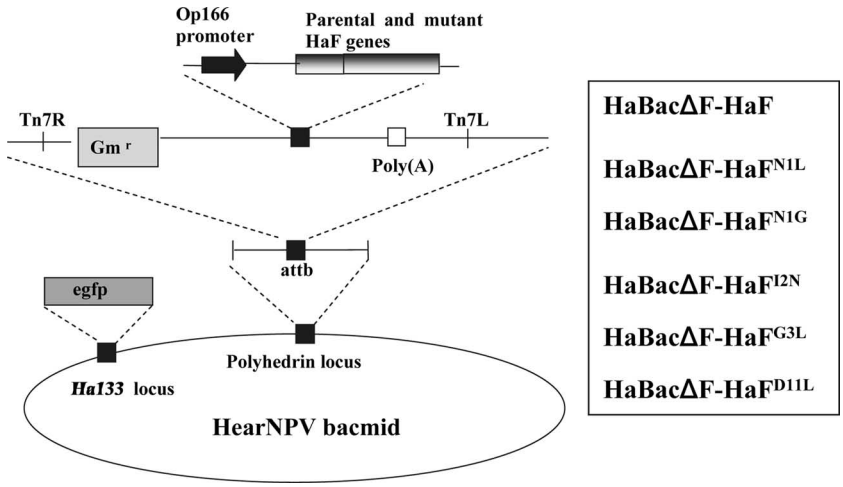

FIG. 3. Strategy for insertion of parental and mutant HaF gene constructs into the polyhedrin locus of the *f*-null HearNPV bacmid. All inserted genes were under the control of the Op166 promoter. All cassettes were inserted into the *attb* site (indicated by right and left insertion sites, Tn*7*R and Tn*7*L) in the polyhedrin locus by transposon-based transposition. The names of recombinant bacmids are listed in the box. *egfp*, enhanced green fluorescent protein.

One-step viral growth curve analyses. Single-step growth curve analyses were conducted on the recombinant viruses, and the results were compared to those for the control virus. HzAM1 cells were infected with each virus at an MOI of 5 $TCID_{50}$ U/cell. Supernatants were harvested at 0, 12, 24, 48, 72, and 96 h postinfection (p.i.) and titrated by end-point dilution assay. Each titration was done in triplicate. The BV titers at different times p.i. were analyzed with one-way analysis of variance (SPSS Inc., 2003) with the virus type as the factor. The average BV titers of the mutants were separated by Fisher's least significant difference test if significant effects were found.

Western blot analysis. The expression of the F proteins and their incorporation into BV were examined by Western blot analysis using polyclonal antibodies against HaF_1. HzAM1 cells were infected with vHaBacΔF-HaF^{N1G}, vHaBacΔF-HaF^{G3L}, and vHaBacΔF-HaF at an MOI of 5 $TCID_{50}$ U/cell. At 4 days p.i., 1 ml of supernatants containing fresh BVs were collected and centrifuged at 3,000 rpm for 5 min to remove cell debris and the virions were pelleted at 12,000 rpm for 30 min at 4°C. The BV pellets were disrupted in 6× sodium dodecyl sulfate (SDS)-polyacrylamide gel electrophoresis sample buffer, separated by 12% SDS-polyacrylamide gel electrophoresis, and transferred onto Hybond-N membranes (Amersham) by semidry electrophoresis (1). Western blot analyses were performed with 1:1,000 dilutions of anti-HaF_1 and anti-VP80 polyclonal antibodies (10) as primary antibodies and alkaline phosphatase-conjugated goat anti-rabbit as secondary antibody (NovoGene Biosciences, China). The signals were detected by using nitroblue tetrazolium–5-bromo-4-chloro-3-indolyl phosphate (SABC, China).

Low-pH-induced envelope fusion assay. The syncytium-forming abilities of the recombinant viruses were tested according to the method of Blissard and Wenz (3) with a slight modification. Briefly, HzAM1 cells were infected with recombinant viruses at an MOI of 5 $TCID_{50}$ U/cell. At 48 h p.i., the cells were washed three times with Grace's medium and then treated with an acidic Grace's insect medium (pH 4.8) for 5 min. The cells were further cultured with normal Grace's insect medium containing 10% fetal bovine serum. Syncytium formation was observed by fluorescence microscopy at 24 h after the acid pH shift and quantified according to the method of Pearson et al. (39). The number of fused cells containing four or more nuclei in five different fields of each sample were counted. The data on the different viruses were compared by Kruskal-Wallis one-way analysis of variance, and the difference between each pair of viruses was determined by Dunn's multiple comparison test.

Analysis of the structure of the fusion peptide of HaF by NMR. To study the structure by NMR, the fusion peptide (NIGLNFVGSVDKFLFGVMDA) of the HaF protein was synthesized by GL Biochem (Shanghai) Ltd. Its purity and molecular mass were assessed by electrospray mass spectrometry, high-performance liquid chromatography, and amino acid analysis. Deuterated SDS was purchased from Cambridge Isotope (Andover, MA). Mixtures of peptides and SDS were sonicated for 30 min before measurements to make the solution more homogeneous and to mimic the membrane environment in vivo.

NMR measurements were carried out at 27°C on a Varian INOVA 600 spectrometer. The NMR sample contained 2 mM fusion peptide, 200 mM D_{25}-SDS in 20 mM phosphate buffer, pH 5.0, with 90% H_2O and 10% D_2O (vol/vol). All of the chemical shifts were externally referenced to the methyl resonance of sodium 2,2-dimethyl-2-silapentane-5-sulfonate (DSS) (0 ppm). WATERGATE (31) was employed for solvent suppression at the end of all the two-dimensional experiments. Total correlation spectroscopy (TOCSY) and nuclear Overhauser effect spectroscopy (NOESY) (4) experiment results were collected in the phase-sensitive detection mode using standard pulse sequence. The data were processed using NMRPipe (9) and analyzed with the XEASY module of the Cara program, version 2.1 (2). Proton resonance assignments were determined from TOCSY at mixing times of 30 ms and 80 ms and NOESY at a mixing time of 300 ms.

For structure calculation, the distance constraints of the fusion peptide in SDS micelles were defined from the NOESY spectrum recorded at the mixing time of 80 ms by using the program CALIBA. Backbone dihedral angle constraints were derived from all the proton chemical shifts by using TALOS (8). A family of 200 structures were calculated with the DYANA (15) program starting from randomly generated conformers in 10,000 annealing steps. Twenty conformers with minimal target functions were subjected to energy minimization using the AMBER force field and chosen for further analysis to represent the structure of the fusion peptide in SDS micelles, with no NOE violations of >0.3 angstroms, no dihedral angle violations of >2.5°, and no van de Walls violations of >0.3 angstroms. The quality of the calculated structures was analyzed by using PROCHECK-NMR (34). The figures and graphical analyses of the peptide structure were created by using MOLMOL (version 2.2) (27) and PyMol (DeLano Scientific, Ltd).

Small molecule structure accession number. The coordinates (code 20026) have been deposited in SMSDep at the Biological Magnetic Resonance Data Bank.

RESULTS

Production of infectious budded virus is compromised by N^1L, I^2N, and $D^{11}L$ mutations. To examine the requirement of the fusion peptide of HaF for certain amino acids, mutated HaFs HaF^{N1G}, HaF^{N1L}, HaF^{I2N}, HaF^{G3L}, and HaF^{D11L} were generated as described in Materials and Methods. All the mutations were verified by nucleotide sequencing. The parental HaF and all the mutated HaFs were inserted into an *f*-null HearNPV bacmid, and the recombinant bacmids HaBacΔF-HaF, HaBacΔF-HaF^{N1L}, HaBacΔF-HaF^{N1G}, HaBacΔF-HaF^{I2N}, HaBacΔF-HaF^{G3L}, and HaBacΔF-HaF^{D11L} were

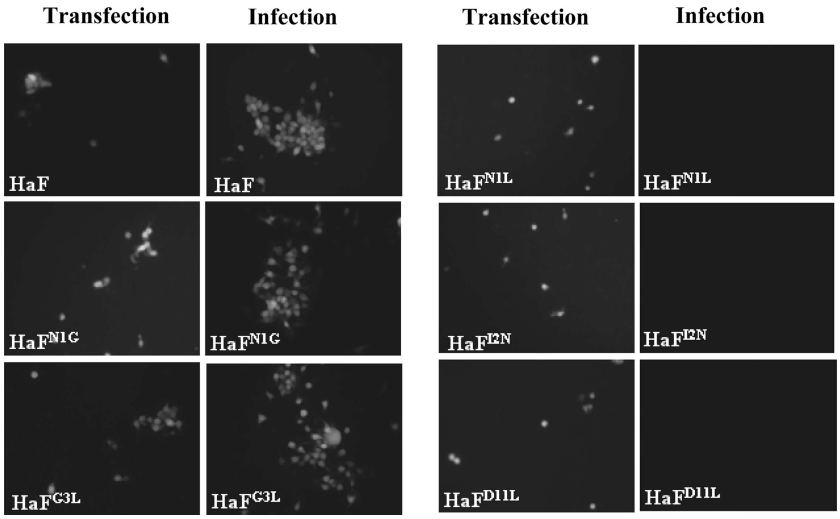

FIG. 4. Results of transfection-infection assay for viral propagation. HzAm1 cells were transfected with *f*-null HearNPV bacmid with various mutant HaFs and parental HaF inserted, incubated for 5 days, and observed under a fluorescence microscope at 5 days p.t. Supernatants from the transfected cells were used to infect HzAM1 cells, and the infected cells were observed under a fluorescence microscope at 4 days p.i.

generated (Fig. 3). All the bacmids were authenticated by PCR and restriction enzyme analyses (data not shown).

Transfection and infection assays were conducted as outlined in Materials and Methods. The data in Fig. 4 show that at 5 days p.t., the presence of green fluorescence was detected in Sf9 cells transfected with recombinant bacmids containing parental HaF and various mutant HaFs, respectively. At 4 days p.i., enhanced green fluorescent protein expression was evident in cells infected with vHaBacΔF-HaF, vHaBacΔF-HaF^{N1G}, and vHaBacΔF-HaF^{G3L}, but not in cells infected with vHaBacΔF-HaF^{N1L}, vHaBacΔF-HaF^{I2N}, and vHaBacΔF-HaF^{D11L}. The results demonstrate that the hydrophobic or hydrophilic property of the amino acids N^1, I^2, and D^{11} is important, as they cannot be functionally replaced by the amino acids with an opposite property (L^1, N^2, and L^{11}).

vHaBacΔF-HaF^{N1G} and vHaBacΔF-HaF^{G3L} produced infectious BV, and their F proteins were properly cleaved. As vHaBacΔF-HaF^{N1G} and vHaBacΔF-HaF^{G3L} appeared to produce infective BV (Fig. 4), one-step growth curve assays of vHaBacΔF-HaF^{N1G}, vHaBacΔF-HaF^{G3L}, and vHaBacΔF-HaF

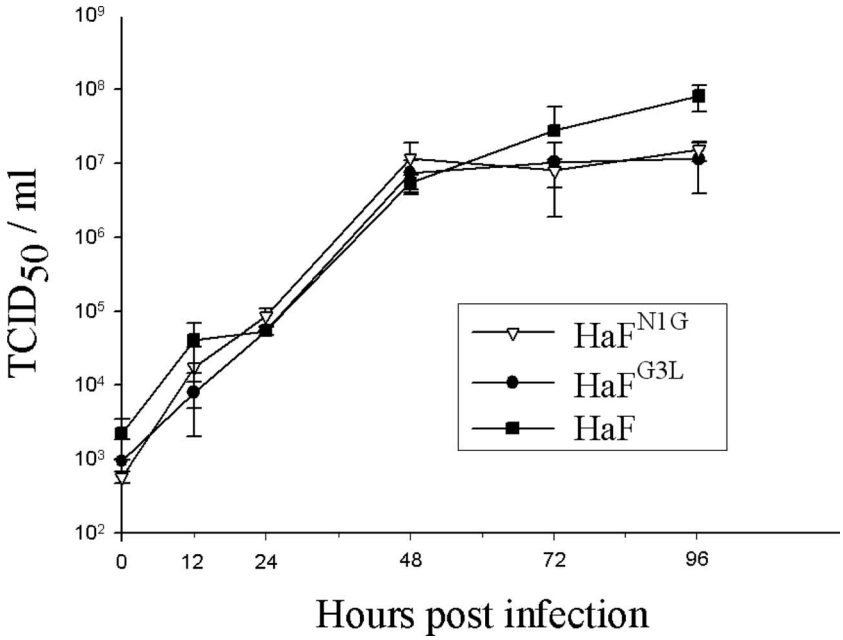

FIG. 5. One-step growth curves of recombinant and control viruses. HzAM1 cells were infected at an MOI of 5 $TCID_{50}$ U/cell with vHaBacΔF-HaF^{N1G}, vHaBacΔF-HaF^{G3L}, and vHaBacΔF-HaF. Cell-free medium was harvested at various times p.i., and the titers of progeny virus were determined by an endpoint dilution assay. Data points represent mean titrations from triplicate infections, and error bars represent standard deviation from the means.

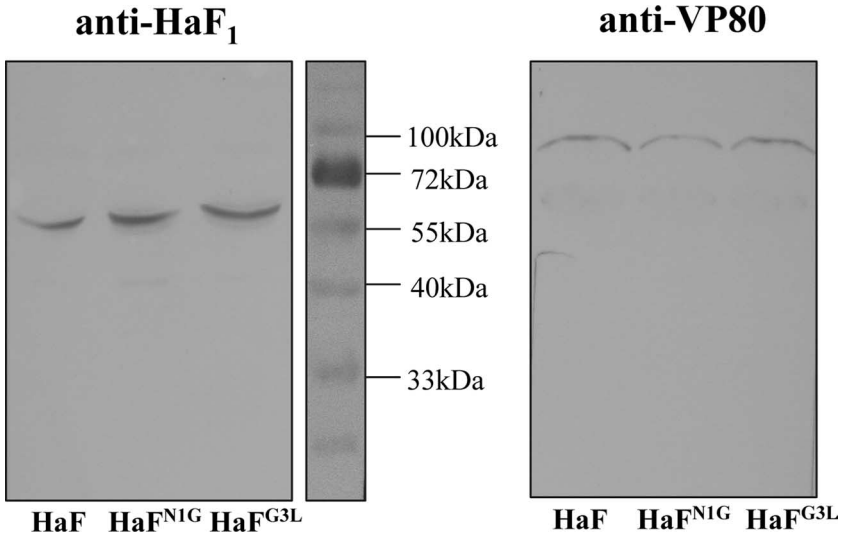

FIG. 6. Western blot analyses of recombinant HearNPV BVs with indicated HaF mutants. HzAm1 cells were infected with vHaBacΔF-HaF^{N1G}, vHaBacΔF-HaF^{G3L}, and vHaBacΔF-HaF at an MOI of 5 $TCID_{50}$ U/cell. BVs were harvested from supernatants, and Western blot analyses were performed by using antibodies against HaF_1 (left) and VP80 (right), respectively.

were performed to analyze the effect of mutations on BV production. HzAM1 cells were infected at an MOI of 5 $TCID_{50}$ U/cell, and cell-free media were harvested at various times p.i. The titers of progeny virus were determined by end-point dilution assay. The data presented in Fig. 5 show that the three viruses had similar kinetics of BV production before 72 h p.i. ($P > 0.05$). However, at the very late stage, e.g., at 96 h p.i., the BV titer of vHaBacΔF-HaF was 8.06×10^7 $TCID_{50}$ U/ml, which was higher than the BV titers of vHaBacΔF-HaF^{N1G} (1.51×10^7 $TCID_{50}$ U/ml) ($F = 17.00$; degree of freedom [*df*] = 1.6; $P = 0.004$), and vHaBacΔF-HaF^{G3L} (1.14×10^7 $TCID_{50}$ U/ml) ($F = 17.00$; $df = 1.6$; $P = 0.002$), while the BV titers of vHaBacΔF-HaF^{N1G} and vHaBacΔF-HaF^{G3L} were not significantly different from each other ($F = 17.00$; $df = 1.6$; $P = 0.347$).

Western blot analyses were conducted with an antibody against HaF_1 to detect the incorporation and cleavage of the recombinant HaFs in progeny BVs. An antibody against the nucleocapsid protein (anti-VP80) was used as an internal control to determine the amount of BVs (Fig. 6). It was shown that the amounts of BVs produced from vHaBacΔF-HaF^{N1G} and vHaBacΔF-HaF^{G3L} were similar to the amount produced from vHaBacΔF-HaF. Bands corresponding to a protein with the predicted molecular size of the HaF_1 subunit (approximately 59 kDa) were detected with the anti-HaF_1 antibody for vHaBacΔF-HaF^{N1G}, vHaBacΔF-HaF^{G3L}, and vHaBacΔF-HaF, and all appeared to exhibit equivalent amounts (Fig. 6). Therefore, HaF^{N1G} and HaF^{G3L} were properly cleaved in infected cells and were efficiently incorporated into BVs similarly to the parental HaF.

The fusion activities of HaF^{N1G} and HaF^{G3L} are different from that of the parental HaF. It was demonstrated that BVs of group II NPVs entered insect host cells via a clathrin-mediated and a low-pH-dependent endocytic route (32). The F protein is responsible for low-pH-dependent cell fusion (22), and fusion peptide is believed to be inserted into the target membrane after exposure to low pH. To characterize the fusion abilities of HaF^{N1G} and HaF^{G3L} in comparison to that of the parental HaF, a syncytium formation assay was performed. The data presented in Fig. 7 show that cell cultures infected with HaBacΔF-HaF^{N1G} showed a significantly higher number of large, multinucleate cells (average, 67 fused cells for five fields in each sample) than cell cultures infected with HaBacΔF-HaF (average, 18 fused cells for five fields in each sample) (Dunn's multiple comparison statistic [Q] = 7.348; $P < 0.05$), while the cell cultures infected with HaBacΔF-HaF^{G3L} had about 38% fewer multinucleate cells (average, 7 fused cells for five fields in each sample) than cell cultures infected with HaBacΔF-HaF ($Q = 3.647$; $P < 0.05$) (Fig. 7). These data indicate that when N^1 was replaced with glycine, the fusion ability of HaF was enhanced, while when hydrophilic G^3 was replaced by hydrophobic leucine, the fusion ability of HaF was reduced.

Structural analysis of the fusion peptide by NMR. NMR structures are usually calculated from a large number of proton-proton distances determined from NOE measurements between protons that are spatially proximal to each other (14). The TOCSY and NOESY spectra of the fusion peptide of HaF in SDS micelles at 300 K in pH 5.0 phosphate buffer were recorded on a Varian 600-MHz spectrometer, and the results displayed numerous well-resolved cross-peaks (Fig. 8A), indicating that the peptide was folded and that assignments should be possible. The NOE connectivities from the NOESY spectrum and chemical shift index of the α-proton are summarized in Fig. 8B. The NOE connectivity of αN (i, i + 3) starts from residue G^3 to G^8 and is slightly interrupted by the absence of αN (N^5, G^8) NOE. The lack of other medium-range NOEs, such as NN (i, i + 2), αN (i, i + 2), and αβ (i, i + 3) from N^1 to G^8 implies a flexible N-terminal fragment, though containing helical structures. A break or loose structure between G^8 and D^{11} would also be expected because of the absence of αN (G^8, D^{11}) NOE. Then, a continuous pattern of αN (i, i + 3) NOEs from S^9 to A^{20} can be seen, and the presence of several NN (i, i + 2), αN (i, i + 2), αN (i, i + 4), and αβ (i, i + 3)

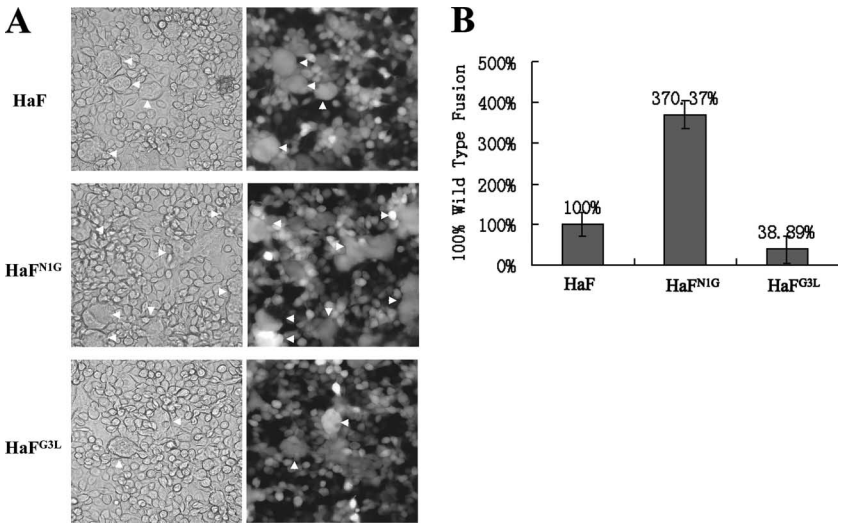

FIG. 7. Syncytium formation analyses. (A) Formation of syncytia induced by HaF and HaF mutants expressed by infected cells. HzAM1 cells were infected with recombinant BVs (vHaBacΔF-HaF^{N1G}, vHaBacΔF-HaF^{G3L}, and vHaBacΔF-HaF) at an MOI of 5 $TCID_{50}$ U/cell. Thirty-six hours after infection, cells were treated for 5 min with Grace's medium at pH 5.0. Syncytium formation was scored 24 h after exposure to acid conditions by phase-contrast microscopy, light (left) and fluorescence (right) micrographs. (B) Quantification of the ability of parental HaF protein and mutant HaF proteins to form syncytia. Each column represents the percentage of parental HaF fusion, and the data are derived from triplicate infection experiments. The error bars represent standard deviations from the means. For details, see Materials and Methods.

NOEs in this region strongly suggests an α-helical structure at the C terminus. The continuous upfield shifts of α-protons from residues N^5 to F^{15} and M^{18} to D^{19} also reveal a stabilization of the α-helical conformation mainly in the middle and C-terminal fragment of the fusion peptide, consistent with the NOE pattern analysis.

A total of 258 nonredundant upper-limit constraints from the assigned NOE cross-peaks were included in the structure calculation together with the TALOS torsion angle constraints. From the initial 100 structures calculated, 20 structures corresponding to those exhibiting the lowest target functions were selected (Fig. 9A). A ribbon representation of the "most typ-

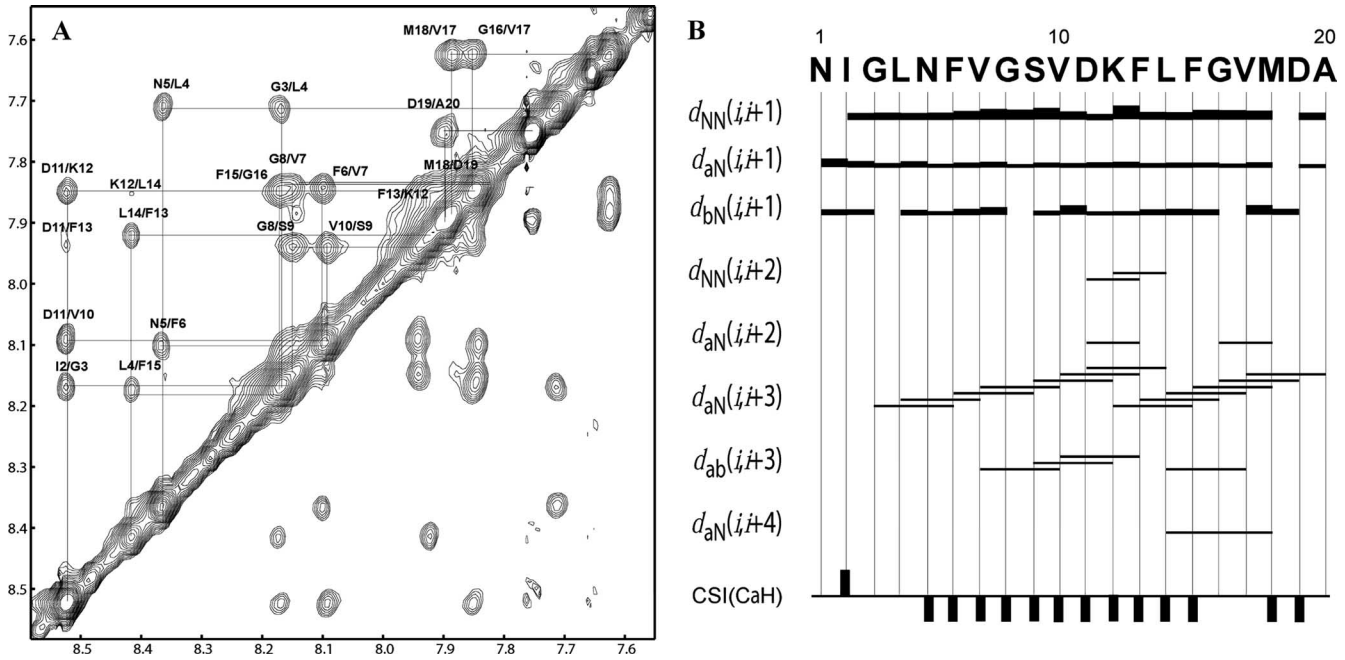

FIG. 8. Secondary structure of the fusion peptide in SDS micelles at pH 5.0, 27°C. (A) Expanded HN/HN region of NOESY spectrum at a mixing time of 300 ms, showing the sequential assignments of all the amide protons. (B) Summary of the NOE connectivities according to NOESY spectrum at 80 ms of mixing time and C^aH chemical shift index (CSI). Bar thickness indicates the intensity of NOE connectivity, with thicker bars representing stronger NOEs. The negative or positive bars in the chemical shift index plot indicate upfield or downfield shifts of more than 0.1 ppm compared with the expected random-coil C^aH value, respectively.

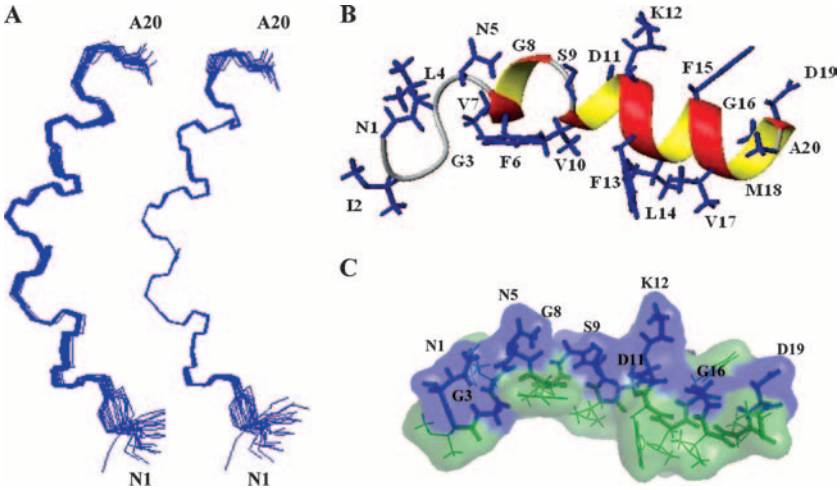

FIG. 9. Structure of the fusion peptide in SDS micelles at pH 5, 27°C by ^{1}H-NMR. (A) Superposition of the backbone atoms of the best 20 structures. The structures are fitted to residues 1 to 20 (left) and residues 7 to 18 (right). (B) Ribbon representation of the structure closest to the mean, with the side chains shown as blue sticks and indicated by residue name and number. (C) Surface representation of the structure closest to the mean, with hydrophilic surface in blue and hydrophobic surface in green. The side chains of hydrophilic residues are shown as blue sticks and indicated by residue name and number.

ical" (closest-to-the-mean) conformer is shown in Fig. 9B, with side chains shown as stick models, and a surface representation with the hydrophilic surface in blue and the hydrophobic surface in green is shown in Fig. 9C). These figures suggest a coil-helix-turn-helix motif for the fusion peptide of HaF at pH 5.0 in a membrane-mimicking environment. The short helix from residue F^6 to residue G^8 is most likely a 3_{10}-helix, while a typical α-helix extends from residue V^{10} to residue D^{19}. Although the ribbon representations of all the 20 structures display a stable α-helix motif at the C terminus, the first loop of this helix is a bit looser, such that the distances between the carbonyls of V^{10} and D^{11} and the amide protons of L^{14} and F^{15} are not small enough to form typical α-helix CO-HN (i, i + 4) hydrogen bonds, while conserved CO-HN (i, i + 4) hydrogen bonds were found from F^{13} to D^{19} in all of the 20 structures. In accordance with our hypothesis, the peptide indeed exhibits highly amphiphilic features, with hydrophobic residues forming a hydrophobic cluster and hydrophilic residues on the other side (Fig. 9B and C), but it is not a continuous α-helix. Interestingly, the best fit of the final set of structures on backbone atoms was found from residues V^7 to M^{18} by the structure statistics given in Table 2, which implies that the hinge of the helix-turn-helix motif at S^9 is quite rigid. This might be important for the peptide to maintain its amphiphilic features.

DISCUSSION

The SDS micelle is quite acceptable to model the membrane bilayer in many studies (13, 21, 23), because the motion of the molecule in the presence of the small micelle is sufficiently fast to allow sharp NMR resonance peaks to be detected (7, 21). Our previous attempt to solve the structure of the fusion peptide of HaF in an aqueous solution at pH 5.0 failed, as the peptide aggregated strongly in the aqueous solution (data not shown). This may be due to self-association driven by the strong hydrophobic interactions among the fusion peptides. Experimental results have shown that the fusion peptide of HaF is well resolved and stable in SDS micelles at pH 5.0; therefore, this membrane-mimicking environment was used in the current study. The NMR solution for the fusion peptide of HaF revealed a structure comprising a flexible coil in the N terminus from N^1 to N^5, a 3_{10}-helix from F^6 to G^8, a turn at S^9, and a regular α-helix from V^{10} to D^{19} (Fig. 9). To our knowledge, this is the first NMR structure of a baculovirus fusion peptide. In the structure, the helix-turn-helix motif from V^7 to M^{18} is quite rigid, suggesting that it is the core structure of the fusion peptide of HaF. This structure is very similar to that of the influenza HA fusion peptide, which is characterized as an angled V or boomerang shape with two helices separated by a 105° kink at pH 5.0 (16, 28). And it has been shown that the

TABLE 2. Structural statistics for the fusion peptide at pH 5.0 (n = 20 structures)[a]

Characteristic	Value
No. of NOE distance restraints	258
Intraresidue	156
Sequential	68
Medium and long range	34
No. of dihedral angle constraints	14
Target function (Å^2)	0.10 ± 0.002
Maximum upper-limit violations (Å)	0.12 ± 0.00
Maximum van der Waals violations (Å)	0.13 ± 0.00
Maximum torsion angle violations (Å)	0.26 ± 0.01
Backbone pairwise RMSD (Å)	
Residues 1–20	0.51
Residues 7–18	0.10
Heavy atom pairwise RMSD (Å)	
Residues 1–20	0.98
Residues 7–18	0.60
Ramachandran plot[b]	
Favored region (%)	100.0
Allowed region (>99.8%)	100.0

[a] None of these structures exhibit distance violations greater than 0.4 Å or dihedral angle violations greater than 4°. Root mean square deviation (RMSD) values are from MOLMOL.

[b] Data are from PROCHECK-NMR.

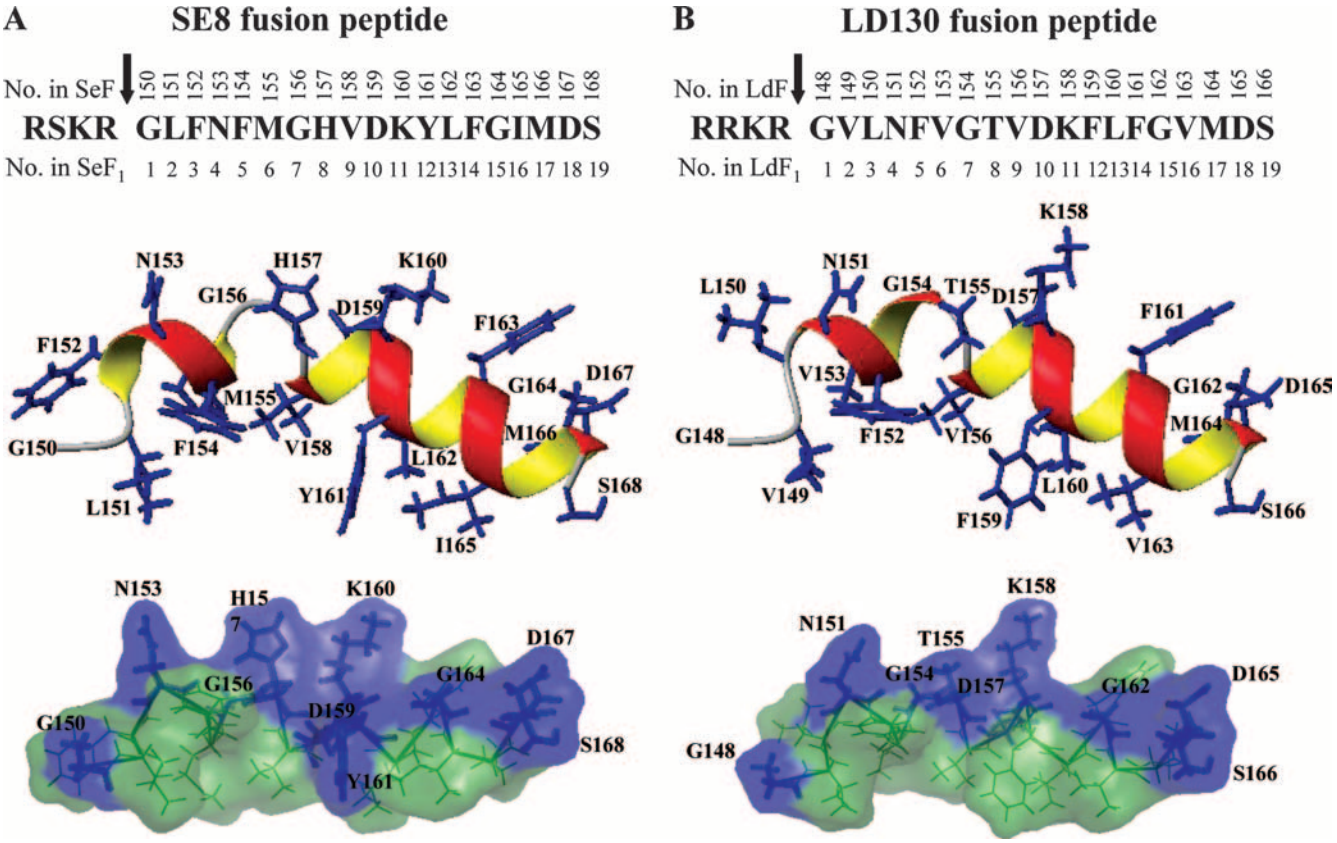

FIG. 10. Computer-assisted modeling of fusion peptides of SE8 (A) and LD130 (B). The predicted structures of the peptides were modeled on the closest-to-mean NMR structure of the fusion peptide of HaF by replacing relevant amino acids using PyMol, followed by energy minimization in Amber force field using Amber version 8.0. Top panels are the linear sequences of the fusion peptides, with the arrows indicating the furin cleavage sites; numbers above the amino acid sequences indicate the residue positions in full-length SE8 (SeF) or LD130 (LdF); numbers beneath the amino acid sequences indicate the residue positions in F_1 fragments of SE8 (SeF_1) or LD130 (LdF_1) starting from the first amino acid of the fusion peptide. Middle panels are ribbon representations, and bottom panels are surface representations with the same color code used in Fig. 9.

kink structure of the influenza HA fusion peptide is essential for its function (28). So far, structural information for many fusion peptides has been revealed by a variety of spectroscopic and computational methods. The HIV gp41 fusion peptide was shown to form an α-helix in membrane-mimicking environments (23, 30, 42). The three-dimensional structure of the Ebola fusion peptide displays a 3_{10}-helix in the central part of the molecule (13). The fusion peptide of the parainfluenza virus 5 F protein adopts a partly extended, partly β-sheet, and partly α-helical prefusion conformation (54). It seems that most fusion peptides prefer to be α-helical when inserted into membranes, since the insertion of amide groups into membranes is energetically highly unfavorable (53). Therefore, it is not unanticipated that our NMR results show that the fusion peptide of HaF also adopts a mainly α-helical structure at pH 5.0 in a membrane-mimetic environment.

A useful strategy to better understand the functional and structural role of the fusion peptide is to compare the effects of the mutant peptides with that of the wild-type peptide in the virus. With the NMR results for the fusion peptide of HaF, we were also able to simulate the structures of the other fusion peptides of group II NPVs to analyze the location of each amino acid. Three-dimensional structures of the fusion peptides of LD130 and SE8 were constructed based on the closest-to-mean NMR structure of the fusion peptide of HaF by replacing relevant amino acids using PyMol, followed by a 10,000-step energy minimization in the Amber force field by Amber version 8.0 (6). The predicted structures of the fusion peptides of SE8 and LD130, which adopted kinked amphiphilic helices similar to those of HaF but with longer N-terminal helices, are shown in Fig. 10. With these structures, we are now able to analyze all the single-amino acid mutations and their biological implications.

The first few residues of the fusion peptide of HaF are not very conserved in group II NPV fusion peptides (Fig. 1), and the NMR results indicated that N^1 to N^5 formed a flexible coil (Fig. 9). A similar but shorter coil is formed by G^{150} to L^{151} in SE8 and by G^{148} to L^{150} in LD130 (Fig. 10). This region may contribute to the function of initial insertion into the membrane and, most likely, into the polar headgroup region of the bilayer. It has been demonstrated that the first residue of the fusion peptide in influenza HA is critical for the fusion reaction, and single-amino acid changes at this position have dramatic effects on its structure (29). Therefore, it is not surprising that the HaF^{N1L} mutant resulted in completely abolished budded-virus production. Replacement of the first asparagine with

glycine (HaF^{N1G}) resulted in enhanced fusion activity and slightly reduced infectious BV production. Both glycine and asparagine share uncharged polar side chains, and since glycine is smaller and more flexible, it may be more beneficial for the initial insertion. This coincides with the fact that the fusion peptides of the other group II NPVs all share glycine as the first residue. The NMR structure of the fusion peptide of HaF shows that the second residue, isoleucine, is extruded in the hydrophobic side of the N-coil. The quenched activity of the HaF^{I2N} mutant suggested that the isoleucine plays an important role in maintaining the structure and balancing the hydrophobic/hydrophilic properties. The HaF^{G3L} mutant had a decreased but still notable fusion activity. Glycine is the smallest amino acid and normally fits into a tight space in a peptide or protein, while leucine, with its relative large side chain, may have a stereo effect on the neighboring residues, so it is understandable that the replacement of the glycine with hydrophobic leucine slightly reduces the bioactivity of the fusion peptide. L^{151} of the fusion peptide of SE8 was simulated to be near the N-coil (Fig. 10), and it could be converted to arginine without notable effect (50), again reflecting the flexibility of this region.

Our NMR results have shown a 3_{10}-helix from F^6 to G^8, and this region is conserved in most group II fusion peptides (Fig. 1), indicating the importance of the structure. The modeled structure of the fusion peptide of SE8 exhibited a longer N-terminal helix from F^{152} to M^{155} (Fig. 10). Westenberg et al. have performed mutational analyses in this region (50), and their results showed that residue F^{152} of the fusion peptide of SE8 could not be replaced by arginine, demonstrating the importance of hydrophobicity at this location. It was also shown that the bacmid with $SE8^{M155R}$ was able to produce infectious virus but impaired in its virus propagation dynamics (50).

In our NMR results, the two helices of the fusion peptide of HaF are separated by a turn of S^9 and a loose head of the C-terminal α-helix which should be able to hold the helices in proper conformation. Correspondingly, G^{156} and $H^{157}$of the fusion peptide of SE8 constituted this turn or bend structure (Fig. 10). Westenberg et al. converted G^{156} of SE8 to alanine, and the results showed no notable effect, suggesting that alanine, slightly more hydrophobic than glycine, can also maintain the structure (50). It has been found that the glycine-to-alanine substitutions have no effect on fusion activity in other viral fusion peptides (20, 41).

The regular α-helix from V^{10} to D^{19} of the fusion peptide of HaF is well conserved in group II NPVs (Fig. 1 and Fig. 10), and this region is likely to be the functional region of the baculovirus fusion peptide. It is therefore not surprising to see that the $D^{11}L$ mutation of HaF abolished the function of HaF (Fig. 4). These observations can also explain why the $K^{158}A$, $D^{165}G$, and $D^{168}G$ mutations of LD130 all resulted in significant reduction of the fusogenicity of the mutated LD130s (39). Similarly, the $V^{158}R$, $K^{160}L$, and $F^{163}R$ mutants of the fusion peptide of SE8 were functional but had impaired recombinant-virus propagation (50). According to our NMR results, the C-terminal α-helix of the fusion peptide is quite rigid; surprisingly, M^{166} of the fusion peptide of SE8 could be converted to arginine without notable effect (50). Further investigations, especially of the structure of the mutant fusion peptides, may provide new insight into the structures.

In summary, our structure-function analysis associating the results of mutagenetic analysis with structural information from NMR elucidates features essential for the fusion activities of group II NPV fusion peptides: (i) the flexible N-terminal coil region and (ii) the principal functional part consisting of a 3_{10}-helix–turn–α-helix. Any mutations altering this stable structure could have discernible effects on the fusion ability. Further investigations are needed to fully understand the fusion process, especially the interaction between the fusion peptide and lipid bilayers, the insertion depth, and the orientation of the peptide. In addition, we need to keep in mind that the fusion peptide is only one segment of the whole fusion protein and that the function of the fusion protein is related to many other factors. Our comparison of fusion abilities and viral growth curves showed that fusion ability might not always correlate to the level of BV production. For example, the HaF^{N1G}-transformed HearNPV with higher fusion ability produced fewer infectious BVs at the late stage of infection than vHaBacΔF-HaF. Probably the mutant fusion peptide had somehow influenced the conformational structure of the whole fusion protein. In order to entirely understand the complexity of the process, we have planned further investigations of the conformation of the baculovirus fusion protein.

ACKNOWLEDGMENTS

This work was supported by NSFC grants (30470076, 30630002, 30670078, 20605026, and 20635040), National Basic Research Program of China (973 program) grant 2003CB114202, and a PSA project grant from MOST and KNAW (2004CB720404).

We thank Basil M. Arif for scientific editing of the manuscript, Xiulian Sun for statistical analysis, Yanfang Zhang for cell culture, and Lingyun Wang for computer-assisted analysis of the fusion peptides of SE8 and LD130.

REFERENCES

1. **Ausubel, F. M., R. Brent, R. E. Kingston, D. D. Moore, J. G. Seidman, J. A. Smith, and K. Struhl.** 1994. Current protocols in molecular biology. J. Wiley and Sons, New York, NY.
2. **Bartels, C., T.-H. Xia, M. Billeter, P. Guntert, and K. Wuthrich.** 1995. The program XEASY for computer-supported NMR spectral analysis of biological macromolecules. J. Biomol. NMR **6:**1–10.
3. **Blissard, G. W., and J. R. Wenz.** 1992. Baculovirus gp64 envelope glycoprotein is sufficient to mediate pH-dependent membrane fusion. J. Virol. **66:**6829–6835.
4. **Braun, S., H. O. Kalinowski, and S. Berger.** 1998. 150 and more basic NMR experiments, 2nd ed. Wiley-VCH, Weinheim, Germany.
5. **Bulach, D. M., C. A. Kumar, A. Zaia, B. Liang, and D. E. Tribe.** 1999. Group II nucleopolyhedrovirus subgroups revealed by phylogenetic analysis of polyhedrin and DNA polymerase gene sequences. J. Invertebr. Pathol. **73:**59–73.
6. **Case, D. A., T. A. Darden, T. E. Cheatham III, C. L. Simmerling, J. Wang, R. E. Duke, R. Luo, K. M. Merz, B. Wang, D. A. Pearlman, M. Crowley, S. Brozell, V. Tsui, H. Gohlke, J. Mongan, V. Hornak, G. Cui, P. Beroza, C. Schafmeister, J. W. Caldwell, W. S. Ross, and P. A. Kollman.** 2004. AMBER 8. University of California, San Francisco, CA.
7. **Chang, D. K., S. F. Cheng, and W. J. Chien.** 1997. The amino-terminal fusion domain peptide of human immunodeficiency virus type 1 gp41 inserts into the sodium dodecyl sulfate micelle primarily as a helix with a conserved glycine at the micelle-water interface. J. Virol. **71:**6593–6602.
8. **Cornilescu, G., F. Delaglio, and A. Bax.** 1999. Protein backbone angle restraints from searching a database for chemical shift and sequence homology. J. Biomol. NMR **13:**289–302.
9. **Delaglio, F., S. Grzesiek, G. W. Vuister, G. Zhu, J. Pfeifer, and A. Bax.** 1995. NMRPipe: a multidimensional spectral processing system based on UNIX pipes. J. Biomol. NMR **6:**277–293.
10. **Deng, F., R. Wang, M. Fang, Y. Jiang, X. Xu, H. Wang, X. Chen, B. M. Arif, L. Guo, H. Wang, and Z. Hu.** 2007. Proteomics analysis of *Helicoverpa armigera* single nucleocapsid nucleopolyhedrovirus identified two new occlusion-derived virus-associated proteins, HA44 and HA100. J. Virol. **81:**9377–9385.

11. **Dutch, R. E., T. S. Jardetzky, and R. A. Lamb.** 2000. Virus membrane fusion proteins: biological machines that undergo a metamorphosis. Biosci Rep. **20:**597–612.
12. **Epand, R. M.** 2003. Fusion peptides and the mechanism of viral fusion. Biochim. Biophys. Acta **1614:**116–121.
13. **Freitas, M. S., L. P. Gaspar, M. Lorenzoni, F. C. L. Almeida, L. W. Tinoco, M. S. Almeida, L. F. Maia, L. Degreve, A. P. Valente, and J. L. Silva.** 2007. Structure of the Ebola fusion peptide in a membrane-mimetic environment and the interaction with lipid rafts. J. Biol. Chem. **282:**27306–27314.
14. **Friebolin, H.** 1991. Basic one- and two-dimensional NMR spectroscopy. VCH, New York, NY.
15. **Güntert, P., C. Mumenthaler, and K. Wüthrich.** 1997. Torsion angle dynamics for NMR structure calculation with the new program DYANA. J. Mol. Biol. **273:**283–298.
16. **Han, X., J. H. Bushweller, D. S. Cafiso, and L. K. Tamm.** 2001. Membrane structure and fusion-triggering conformational change of the fusion domain from influenza hemagglutinin. Nat. Struct. Biol. **8:**715–720.
17. **Hefferon, K. L., A. G. P. Oomens, S. A. Monsma, C. M. Finnerty, and G. W. Blissard.** 1999. Host cell receptor binding by baculovirus GP64 and kinetics of virion entry. Virology **258:**455–468.
18. **Herniou, E. A., T. Luque, X. Chen, J. M. Vlak, D. Winstanley, J. S. Cory, and D. R. O'Reilly.** 2001. Use of whole genome sequence data to infer baculovirus phylogeny. J. Virol. **75:**8117–8126.
19. **Ho, S. N., H. D. Hunt, R. M. Horton, J. K. Pullen, and L. R. Pease.** 1989. Site-directed mutagenesis by overlap extension using the polymerase chain reaction. Gene **77:**51–59.
20. **Horvath, C. M., and R. A. Lamb.** 1992. Studies on the fusion peptide of a paramyxovirus fusion glycoprotein: roles of conserved residues in cell fusion. J. Virol. **66:**2443–2455.
21. **Hsu, C. H., S. H. Wu, D. K. Chang, and C. Chen.** 2002. Structural characterizations of fusion peptide analogs of influenza virus hemagglutinin. Implication of the necessity of a helix-hinge-helix motif in fusion activity. J. Biol. Chem. **277:**22725–22733.
22. **Ijkel, W. F. J., M. Westenberg, R. W. Goldbach, G. W. Blissard, J. M. Vlak, and D. Zuidema.** 2000. A novel baculovirus envelope fusion protein with a proprotein convertase cleavage site. Virology **275:**30–41.
23. **Jaroniec, C. P., J. D. Kaufman, S. J. Stahl, M. Viard, R. Blumenthal, P. T. Wingfield, and A. Bax.** 2005. Structure and dynamics of micelle-associated human immunodeficiency virus gp41 fusion domain. Biochemistry **44:**16167–16180.
24. **Kielian, M.** 2006. Class II virus membrane fusion proteins. Virology **344:**38–47.
25. **Kielian, M., and S. Jungerwirth.** 1990. Mechanisms of enveloped virus entry into cells. Mol. Biol. Med. **7:**17–31.
26. **Klasse, P. J., R. Bron, and M. Marsh.** 1998. Mechanisms of enveloped virus entry into animal cells. Adv. Drug Deliv. Rev. **34:**65–91.
27. **Koradi, R., M. Billeter, and K. Wüthrich.** 1996. MOLMOL: a program for display and analysis of macromolecular structures. J. Mol. Graph. **14:**51–55.
28. **Lai, A. L., H. Park, J. M. White, and L. K. Tamm.** 2006. Fusion peptide of influenza hemagglutinin requires a fixed angle boomerang structure for activity. J. Biol. Chem. **281:**5760–5770.
29. **Li, Y., X. Han, A. L. Lai, J. H. Bushweller, D. S. Cafiso, and L. K. Tamm.** 2005. Membrane structures of the hemifusion-inducing fusion peptide mutant G1S and the fusion-blocking mutant G1V of influenza virus hemagglutinin suggest a mechanism for pore opening in membrane fusion. J. Virol. **79:**12065–12076.
30. **Li, Y., and L. K. Tamm.** 2007. Structure and plasticity of the human immunodeficiency virus gp41 fusion domain in lipid micelles and bilayers. Biophys. J. **93:**876–885.
31. **Liu, M., X. Mao, C. Ye, H. Huang, J. K. Nicholson, and J. C. Lindon.** 1998. Improved WATERGATE pulse sequences for solvent suppression in NMR spectroscopy. J. Magn. Reson. **132:**125–129.
32. **Long, G., X. Pan, R. Kormelink, and J. M. Vlak.** 2006. Functional entry of baculovirus into insect and mammalian cells is dependent on clathrin-mediated endocytosis. J. Virol. **80:**8830–8833.
33. **Long, G., M. Westenberg, H. Wang, J. M. Vlak, and Z. Hu.** 2006. Function, oligomerization and N-linked glycosylation of the *Helicoverpa armigera* single nucleopolyhedrovirus envelope fusion protein. J. Gen. Virol. **87:**839–846.
34. **Lovell, S. C., I. W. Davis, W. B. Arendall III, P. I. W. de Bakker, J. M. Word, M. G. Prisant, J. S. Richardson, and D. C. Richardson.** 2003. Structure validation by Calpha geometry: phi, psi and Cbeta deviation. Proteins **50:**437–450.
35. **McIntosh, A. H., and C. M. Ignoffo.** 1983. Characterization of five cell lines established from species of Heliothis. Appl. Entomol Zool. **18:**262–269.
36. **Monsma, S. A., and G. W. Blissard.** 1995. Identification of a membrane fusion domain and an oligomerization domain in the baculovirus GP64 envelope fusion protein. J. Virol. **69:**2583–2595.
37. **Oomens, A. G. P., and G. W. Blissard.** 1999. Requirement for GP64 to drive efficient budding of Autographa californica multicapsid nucleopolyhedrovirus. Virology **15:**297–314.
38. **Pearson, M. N., C. Groten, and G. F. Rohrmann.** 2000. Identification of the *Lymantria dispar* nucleopolyhedrovirus envelope fusion protein provides evidence for a phylogenetic division of the *Baculoviridae*. J. Virol. **74:**6126–6131.
39. **Pearson, M. N., R. L. Q. Russell, and G. F. Rohrmann.** 2002. Functional analysis of a conserved region of the baculovirus envelope fusion protein, LD130. Virology **304:**81–88.
40. **Qiao, H., R. T. Armstrong, G. B. Melikyan, F. S. Cohen, and J. M. White.** 1999. A specific point mutant at position 1 of the influenza hemagglutinin fusion peptide displays a hemifusion phenotype. Mol. Biol. Cell **10:**2759–2769.
41. **Russell, C. J., T. S. Jardetzky, and R. A. Lamb.** 2004. Conserved glycine residues in the fusion peptide of the paramyxovirus fusion protein regulate activation of the native state. J. Virol. **78:**13727–13742.
42. **Sackett, K., and Y. Shai.** 2005. The HIV fusion peptide adopts intermolecular parallel beta-sheet structure in membranes when stabilized by the adjacent N-terminal heptad repeat: a ^{13}C FTIR study. J. Mol. Biol. **350:**790–805.
43. **Sollner, T. H.** 2004. Intracellular and viral membrane fusion: a uniting mechanism. Curr. Opin. Cell Biol. **16:**429–435.
44. **Tamm, L. K., J. Crane, and V. Kiessling.** 2003. Membrane fusion: a structural perspective on the interplay of lipids and proteins. Curr. Opin. Struct. Biol. **13:**453–466.
45. **Tamm, L. K., X. Han, Y. Li, and A. L. Lai.** 2002. Structure and function of membrane fusion peptides. Biopolymers **66:**249–260.
46. **Wang, H., F. Deng, G. P. Pijlman, X. Chen, X. Sun, J. M. Vlak, and Z. Hu.** 2003. Cloning of biologically active genomes from a *Helicoverpa armigera* single-nucleocapsid nucleopolyhedrovirus isolate by using a bacterial artificial chromosome. Virus Res. **97:**57–63.
47. **Wang, M., Y. Tan, F. Yin, F. Deng, J. M. Vlak, Z. Hu, and H. Wang.** 2008. The F protein of *Helicoverpa armigera* single nucleopolyhedrovirus can be substituted functionally with its homologue from *Spodoptera exigua* multiple nucleopolyhedrovirus. J. Gen. Virol. **89:**791–798.
48. **Weissenhorna, W., A. Hinza, and Y. Gaudin.** 2007. Virus membrane fusion. FEBS Lett. **581:**2150–2155.
49. **Westenberg, M., P. Uijtdewilligen, and J. M. Vlak.** 2007. Baculovirus envelope fusion proteins F and GP64 exploit distinct receptors to gain entry into cultured insect cells. J. Gen. Virol. **88:**3302–3306.
50. **Westenberg, M., F. Veenman, E. C. Roode, R. W. Goldbach, J. M. Vlak, and D. Zuidema.** 2004. Functional analysis of the putative fusion domain of the baculovirus envelope fusion protein F. J. Virol. **78:**6946–6954.
51. **Westenberg, M., H. Wang, W. F. J. Ijkel, R. W. Goldbach, J. M. Vlak, and D. Zuidema.** 2002. Furin is involved in baculovirus envelope fusion protein activation. J. Virol. **76:**178–184.
52. **White, J. M.** 1992. Membrane fusion. Science **258:**917–924.
53. **Wimley, W. C., and S. H. White.** 1996. Experimentally determined hydrophobicity scale for proteins at membrane interfaces. Nat. Struct. Biol. **3:**842–848.
54. **Yin, H. S., X. Wen, R. G. Paterson, R. A. Lamb, and T. S. Jardetzky.** 2006. Structure of the parainfluenza virus 5 F protein in its metastable, prefusion conformation. Nature **439:**38–44.
55. **Zanotto, P. M., M. J. Sampaio, D. W. Johnson, T. L. Rocha, and J. E. Maruniak.** 1992. The Anticarsia gemmatalis nuclear polyhedrosis virus polyhedrin gene region: sequence analysis, gene product and structural comparisons. J. Gen. Virol. **73:**1049–1056.